

Possible effects of charge frustration in Na_xCoO_2 : bandwidth suppression, charge orders and resurrected RVB superconductivity

O. I. Motrunich and Patrick A. Lee

Department of Physics, Massachusetts Institute of Technology, Cambridge MA 02139

(Dated: October 16, 2003)

Charge frustration due to further neighbor Coulomb repulsion can have dramatic effects on the electronic properties of Na_xCoO_2 in the full doping range. It can significantly reduce the effective mobility of the charge carriers, leading to a low degeneracy temperature $\epsilon_F \lesssim T$. Such strongly renormalized Fermi liquid has rather unusual properties—from the point of view of the ordinary metals with $\epsilon_F \gg T$ —but similar to the properties that are actually observed in the Na_xCoO_2 system. For example, we show that the anomalous thermopower and Hall effect observed in $\text{Na}_{0.7}\text{CoO}_2$ may be interpreted along these lines. If the repulsion is strong, it can also lead to charge order; nevertheless, away from the commensurate dopings, the configurational constraints allow some mobility for the charge carriers, i.e., there remains some “metallic” component. Finally, the particularly strong bandwidth suppression around the commensurate $x = 1/3$ can help resurrect the RVB superconductivity, which would otherwise not be expected near this high doping. These suggestions are demonstrated specifically for a tJ -like model with an additional nearest neighbor repulsion.

I. INTRODUCTION

Recent discovery¹ and confirmation^{2,3,4} of superconductivity in $\text{Na}_{0.35}\text{CoO}_2 \cdot 1.3\text{H}_2\text{O}$ has stimulated many studies of this material, and in particular of its unhydrated precursor host material $\text{Na}_{0.7}\text{CoO}_2$. The Na_xCoO_2 series has been known for more than five years^{5,6,7,8} for its unusual transport properties such as large thermoelectric power and nearly linear- T dependence of the resistivity, indicative of strong correlation effects. This has been brought up even further by a number of recent careful experiments.^{9,10,11,12,13,14}

It appears from these studies^{4,6} that there is a large suppression of the valence band width (equivalently, large effective mass enhancement)—by an order of magnitude compared with the LDA band structure calculations.¹⁵

We suggest that such large renormalization may be caused by strong Coulomb repulsion between charge carriers on neighboring Co sites, and point out that a number of unusual properties of the system may be explained by the resulting low fermion degeneracy temperature. We also consider other possible effects of such repulsion, in particular, charge ordering.

The plan of the paper is as follows. To be specific, we consider a tJ -like model with additional strong nearest neighbor repulsion V . In sections II-V, we concentrate on the dominant t, V energetics. The study is done by considering Gutzwiller-like trial fermionic wavefunctions (projected Fermi liquid) with additional nearest neighbor correlations input through a Jastrow-type configurational weighting factor. The strength of the input correlations serves as a variational parameter.

Sec. III studies the properties of these wavefunctions. We find that up to moderate input correlations, the wavefunction indeed describes a renormalized Fermi liquid, consistent with the initial motivation. We also realize that for strong input correlation and over the doping range $0.27 < x < 0.5$ and $0.5 < x < 0.73$, our Jastrow-

Gutzwiller wavefunction has a $\sqrt{3} \times \sqrt{3}$ charge order, which is inherited from the charge distribution properties of the classical Jastrow weight on the lattice. Since such a state is beyond our initial motivation, we examine its properties and treat it very critically whenever the variational parameter is driven into this regime.

In Sec. IV we develop a convenient renormalized mean-field picture for the energetics in the entire doping range. We identify the regime of the renormalized Fermi liquid state, and also the regime where the strong repulsion drives the optimal Jastrow-Gutzwiller wavefunction into the $\sqrt{3} \times \sqrt{3}$ charge order state.

In Sec. V we confirm the renormalized meanfield picture with numerically accurate evaluations with the trial wavefunctions. We also perform a more detailed study of the possible $\sqrt{3} \times \sqrt{3}$ charge order by comparing with the more conventional CDW states. We find that our Jastrow-Gutzwiller wavefunction in the $\sqrt{3} \times \sqrt{3}$ regime is rather good energetically and suggest some ways for improving the energetics further.

In Sec. VI we add the J term and consider the issue of RVB superconductivity at low dopings. This is done with the help of the renormalized meanfield picture. Without the Jastrow renormalizations, the RVB superconductivity would not survive to the experimentally observed $x = 0.35$. We find that the bandwidth suppression due to charge frustration may indeed resurrect the superconductivity near $x = 1/3$ where such renormalizations are strongest, particularly if we allow the coexisting charge order. We speculate that this may be relevant to explain the narrow doping range in which the superconductivity has been found.³

Finally, in Sec. VII we conclude with some simple predictions for the experiments from the developed charge frustration picture. Most notably, transport properties such as thermopower and Hall effect of the Fermi liquid with low degeneracy temperature resemble those of the $\text{Na}_{0.7}\text{CoO}_2$ system; these properties look rather unusual from the perspective of conventional metals.

Before proceeding, we remark about the possibility of charge order^{8,16} in Na_xCoO_2 . The experimental situation is not settled on this issue.^{12,13,14} We favor the picture where there is no charge order, but only strong local correlations. Charge ordering transition should exhibit itself in an abrupt change in transport properties, which has not been observed.

In the present paper, we do spend a lot of time discussing the particular $\sqrt{3} \times \sqrt{3}$ order, since it inevitably arises in our systematic treatment of the concrete model. We should warn the reader that the details are likely strongly model-dependent. Since we do not know the precise microscopic model, the presented analysis of the charge order should be viewed only as an initial sketch of what might happen. The reported work is done with the nearest neighbor repulsion (and nearest neighbor Jastrow correlation) only. Including further neighbor correlations would frustrate the $\sqrt{3} \times \sqrt{3}$ charge order and extend the renormalized Fermi liquid regime, but might also lead to more complicated charge orders. We have not pursued such studies systematically, concentrating on the nearest neighbor case only.

II. tV MODEL. JASTROW-GUTZWILLER Ψ

For concreteness, we consider the following single band Hubbard model with additional nearest neighbor repulsion¹⁶ on a triangular lattice

$$\hat{H}_{tV} = P_G \sum_{\langle ij \rangle} -(tc_{i\sigma}^\dagger c_{j\sigma} + \text{h.c.}) P_G + V \sum_{\langle ij \rangle} n_i n_j. \quad (1)$$

Large onsite repulsion is taken into account using the Gutzwiller projector P_G to project out double-occupation of sites—this gives the “ t part” as in the familiar tJ Hamiltonian. We focus primarily on the effect of adding strong nearest neighbor charge repulsion V , and refer to Eq. (1) as tV Hamiltonian. (We will consider the full tJV Hamiltonian with $J \ll t, V$ later.) The band is less than half-filled, with the average fermion density $\langle c_{i\sigma}^\dagger c_{i\sigma} \rangle = \rho < 1$.

In the context of the Na_xCoO_2 system, $c_{i\sigma}^\dagger$ creates a spinful hole and represents the motion of a Co^{4+} ($S = 1/2$) site, while Co^{3+} ($S = 0$) sites have no holes; $\rho = 1 - x$. This is shown schematically in Fig. 1. For more details, see also Refs. 17,18,19. We take $t > 0$, as in Refs. 17,19. This is consistent with the photoemission studies,¹¹ and also with the high temperature behavior of the Hall coefficient¹⁰ (see Sec. VII). In this picture the end compound NaCoO_2 consists of all Co^{3+} with no holes ($\rho = 0, x = 1$), whereas the hypothetical end compound $\text{Na}_{x=0}\text{CoO}_2$ consists of a Mott insulator with all Co^{4+} sites each carrying $S = \frac{1}{2}$ ($\rho = 1, x = 0$). From the latter point of view, Na_xCoO_2 can be viewed as electron doping by a concentration of x electrons into a Mott insulator.

Here, in order to gauge the effect of the nearest neighbor repulsion, we perform a trial wavefunction study of

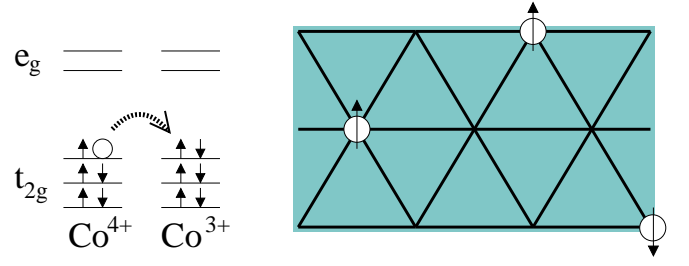


FIG. 1: Na_xCoO_2 : Schematic pictures (borrowed from Ref. 9) explaining the single band electronic model. The charge carriers are spin-1/2 charge $q = |e|$ holes of density $\rho = 1 - x$.

this strongly correlated system. When $V = 0$, a good trial wavefunction is obtained by Gutzwiller-projecting a simple free fermion state:

$$|\Psi_G\rangle = P_G |\Psi_0\rangle = \sum_{\{R\}, \{R'\}} \det[\phi_i(R_j)] c_{R_1\uparrow} \dots c_{R_{N/2}\uparrow} \times \det[\phi_i(R'_j)] c_{R'_1\downarrow} \dots c_{R'_{N/2}\downarrow},$$

where the sum is over all configurations of spin up and down fermions with all R_j and R'_j distinct, $\{R\} \cap \{R'\} = 0$. Away from half-filling, this Gutzwiller wavefunction is a Fermi liquid state; this can be confirmed, e.g., by measuring the quasiparticle Z from the step in $\langle \hat{n}_{\mathbf{k}} \rangle$. In this state, we have approximately $\langle n_i n_j \rangle \approx \rho^2$, while the fermion kinetic energy can be fairly accurately estimated from that of the preprojected free fermions^{20,21,22}

$$\frac{\langle \Psi_G | \hat{H}_t | \Psi_G \rangle}{\langle \Psi_G | \Psi_G \rangle} \approx g_t \frac{\langle \Psi_0 | \hat{H}_t | \Psi_0 \rangle}{\langle \Psi_0 | \Psi_0 \rangle}, \quad (2)$$

with

$$g_t = \frac{1 - \rho}{1 - \rho/2} = \frac{2x}{1 + x}. \quad (3)$$

This is commonly referred to as the Gutzwiller approximation, or the renormalized mean field theory. The renormalization factor g_t can be obtained by counting the number of real space configurations available for hopping in the projected and preprojected states, and ignoring all other wavefunction differences.

Turning on the nearest neighbor repulsion V , we schematize its effect on the ground state by introducing an additional Jastrow-type factor

$$\exp \left[-\frac{W}{2} \sum_{\langle ij \rangle} n_i n_j \right] \quad (4)$$

for each real space configuration of fermions in the above Gutzwiller wavefunction. $W > 0$ effectively suppresses the nearest neighbor occupation probability, and can be varied to optimize the trial energy of the tV Hamiltonian. We will refer to this wavefunction as Jastrow-Gutzwiller (JG) Ψ_{JG} .

It is clear that the effect of V is most severe for $x = 1/3$ and $2/3$. For $V \gg t$ we expect $W \gg 1$, in which case the vacancies (for $x = 1/3$) or the spin carrying holes (for $x = 2/3$) would form a $\sqrt{3} \times \sqrt{3}$ structure to minimize the repulsion. Furthermore in this state the particles cannot hop without paying the energy V . For intermediate V and away from commensuration some remnant of this “jamming” phenomenon may remain and this is what we would like to investigate in this paper.

III. PROPERTIES OF Ψ_{JG} . CLASSICAL LATTICE GAS SYSTEM.

Before presenting the optimized energetics with Ψ_{JG} , we first discuss its properties. For nonzero but small W , it still describes a Fermi liquid state with some further renormalizations compared to the Gutzwiller wavefunction. However, one has to be careful when W becomes large: The probability of finding a particular configuration of charges now has an additional “classical” weight $\exp[-W \sum_{\langle ij \rangle} n_i n_j]$, and one has to be wary of the possibility of phase transitions in the corresponding statistical system. Factoring out many possible spin assignments for each charge configuration, we need to consider a classical system of particles with nearest neighbor repulsion on a triangular lattice with the classical partition function

$$Z_{\text{class}} = \sum_{\{n_i\}} e^{-\mathcal{U}_{\text{class}}[n]} = \sum_{\{n_i\}} e^{-W \sum_{\langle ij \rangle} n_i n_j}. \quad (5)$$

Here $n_i = 0, 1$, and we work at fixed density ρ as appropriate for the discussion of our trial wavefunctions with fixed fermion number. W plays the role of the inverse temperature in this classical system, $W = T^{-1}$ (the classical repulsion strength is set to one).

This lattice gas system has been extensively studied in statistical physics,^{23,24} most notably as a model for adsorbed monolayers of rare-gas atoms on graphite. Also, it is equivalent to a triangular lattice Ising antiferromagnet in an external field; fixed particle density corresponds to fixed magnetization in the Ising system.

The phase diagram in the $\rho - T$ plane is shown in Fig. 2. It is symmetric with respect to $\rho = 0.5$ due to particle-hole symmetry in this classical system, and we discuss the $\rho < 0.5$ part only.

At high temperatures (small W) the system is in a disordered gaseous phase. For small particle density $\rho < 0.27$ the system remains in the gas phase all the way to zero temperature. For densities $0.27 < \rho < 0.5$ the system “crystallizes” into a $\sqrt{3} \times \sqrt{3}$ state at low temperature. This state is characterized by a preferential particle occupation of one of the three sublattices of the triangular lattice; the order is strongest near the commensurate $\rho = 1/3, 2/3$. Note that away from these ρ the $\sqrt{3} \times \sqrt{3}$ phase is more properly characterized as a density wave state rather than a crystal. In particular, a fraction of particles remains relatively mobile having no

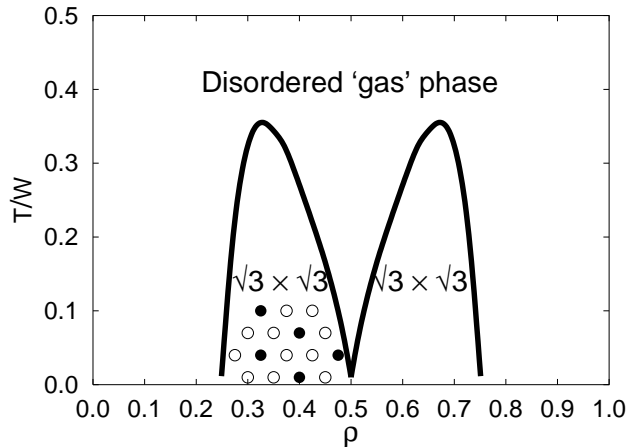


FIG. 2: Phase diagram of the classical lattice gas system Eq. (5). Note the symmetry relative to $\rho = 0.5$ due to particle-hole symmetry.

activation energy for their motion. The $W = \infty$ model is equivalent to the Baxter’s hard hexagon model and is exactly solvable.²⁴

It is useful to have the following caricatures of the charge motion in the $\sqrt{3} \times \sqrt{3}$ phase, appropriate at low temperature (large W) and near the commensurate filling $1/3$. For $\rho > 1/3$, we have one sublattice, say A , completely occupied by particles (these particles are almost localized), while the remaining small density is smeared out relatively uniformly over the honeycomb lattice formed by the B and C sublattices. For $\rho < 1/3$, we picture the B and C sites as completely empty (with almost no density fluctuation), while all particles are spread over the A sublattice. The charge motion is achieved by hops from occupied A sites to neighboring empty A sites via B or C sites; the most effective such hops involve at least two neighboring empty A sites in order to avoid the repulsion energy cost for the intermediate step (see Fig. 8 in Sec. V).

Returning to our trial wavefunction, we expect it to roughly inherit the charge distribution properties of the lattice gas system Eq. (5). Thus, for W such that the classical system is in its disordered phase, the wavefunction realizes a Fermi liquid state. On the other hand, when the classical system is in the $\sqrt{3} \times \sqrt{3}$ phase, we have checked by variational Monte Carlo studies that the resulting wavefunction has a charge density wave (CDW) order but retains some liquid properties. (The transition point W_c is slightly different for the wavefunction and the classical system.) Note that the above Jastrow weight realizes a soft projection satisfying the nearest neighbor repulsion V . It follows that a hard such projection ($W \rightarrow \infty$) leads to the $\sqrt{3} \times \sqrt{3}$ density wave for $0.27 < \rho < 0.5$ and $0.5 < \rho < 0.73$.

Before proceeding further, we want to emphasize again that we set out to study Fermi liquid renormalizations induced by nearest neighbor repulsion. Fermi liquid state

is achieved in the parameter regime where the classical system remains disordered; in this case, our treatment is consistent.

On the other hand, when the nearest neighbor repulsion is strong, it drives the optimal variational parameter W of Ψ_{JG} into the regime with the CDW order. In this case, we have to be very cautious in interpreting the “transition” and the resulting state, since our original assumptions about the properties of the wavefunction no longer hold. We may still interpret this as a sign of an instability towards a different state (most likely with charge order), but the JG wavefunction in this regime should be treated very critically, particularly since it has somewhat unusual charge distribution properties. Thus, one should at least examine other more conventional trial states with different orders. This is done in Sec. V.

IV. ENERGETICS WITH Ψ_{JG} : RENORMALIZED MEANFIELD PICTURE.

We now proceed to the actual energetics with the Jastrow-Gutzwiller trial wavefunctions. It is possible to perform essentially exact evaluations of the expectation values with such fermionic wavefunctions using a well established and documented Variational Monte

Carlo (VMC) procedure.^{21,22,25} Such detailed studies of the tV energetics at experimentally relevant $x = 0.7$ and 0.35 are reported in the next section.

It is also possible to study more complicated Hamiltonians. However, VMC evaluations are computationally rather costly. Furthermore, they become inconclusive when the energy differences become very small. This is particularly the case when we attempt to study the physics at energy scales below the dominant t and V , e.g., if we want to resolve the spin sector, or study pairing instabilities due to the J term.

Useful and fairly accurate guidance is obtained through the following “renormalized meanfield” procedure,^{20,21,22} which is much simpler computationally and is also more amenable to interpretation and extrapolation in the regime where VMC results become inconclusive. Generalization of the configuration counting arguments mentioned earlier leads to the following estimate of the hopping energy renormalization in the JG wavefunction relative to the unprojected free fermion wavefunction:

$$\frac{\langle \Psi_{JG} | c_{i\uparrow}^\dagger c_{j\uparrow} | \Psi_{JG} \rangle}{\langle \Psi_{JG} | \Psi_{JG} \rangle} = g_t[i, j] \frac{\langle \Psi_0 | c_{i\uparrow}^\dagger c_{j\uparrow} | \Psi_0 \rangle}{\langle \Psi_0 | \Psi_0 \rangle} \quad (6)$$

with

$$g_t[i, j] = \frac{1}{\rho(1-\rho/2)} \left\langle \left\langle \delta(n_i - 0) \delta(n_j - 1) \exp \left[-\frac{1}{2} \left(\mathfrak{U}_{\text{class}}[n_i = 1, n_j = 0] - \mathfrak{U}_{\text{class}}[n_i = 0, n_j = 1] \right) \right] \right\rangle \right\rangle. \quad (7)$$

Here, $\langle \dots \rangle$ denotes averaging in the classical lattice gas system with the weight $\sim \exp(-\mathfrak{U}_{\text{class}}[n])$ discussed earlier. When obtaining this expression, similar to the original Gutzwiller approximation Eq. (3), we again ignored the details of the fermionic determinant weighting of configurations, but kept the Jastrow weighting. Only configurations with the occupied j site and unoccupied i site contribute, and the specific “transition weight” comes from the corresponding Jastrow weighting of the configurations before and after the hop. Note that $\mathfrak{U}_{\text{class}}[n_i = 1, n_j = 0] - \mathfrak{U}_{\text{class}}[n_i = 0, n_j = 1]$ is a local energy term involving only the affected sites i, j , and their immediate neighbors.

Similarly, we can approximate the nearest neighbor repulsion energy by

$$\frac{\langle \Psi_{JG} | \hat{n}_i \hat{n}_j | \Psi_{JG} \rangle}{\langle \Psi_{JG} | \Psi_{JG} \rangle} \approx \langle \langle n_i n_j \rangle \rangle. \quad (8)$$

The required classical expectation values are readily evaluated via a Monte Carlo study of the lattice gas system. As we will see in the next section, such renormalized meanfield procedure indeed gives fairly accurate estimates of the expectation values in the Jastrow-Gutzwiller

wavefunction, both in the metallic and the density wave regimes.

We can now develop an overall picture for all fermion densities. Particular cuts through the results are shown in Figs. 3 and 4. Figure 3 shows the hopping renormalization factor g_t as a function of x for a number of fixed W . (Complimentary cuts through the data for the specific fixed $x = 0.70$ and $x = 0.35$ can be also found in the next section.) Figure 3 is the core of the present paper.

The $W = 0$ curve gives precisely the original Gutzwiller approximation Eq. (3) for the no-double-occupancy constraint. This sets a useful reference for gauging the additional effect of the nearest neighbor repulsion. The curve with the largest $W = 8$, on the other hand, essentially realizes a complete projection that satisfies the nearest neighbor repulsion; this is the maximal renormalization that can be achieved with such nearest neighbor correlations. The phase boundary of the classical lattice gas (cf. Fig. 2) is sketched by a thick dark line: All points above the line are in the disordered phase (Fermi liquid wavefunctions), while points below the line are in the $\sqrt{3} \times \sqrt{3}$ density wave phase.

Figure 4 shows a similar plot for the repulsion en-

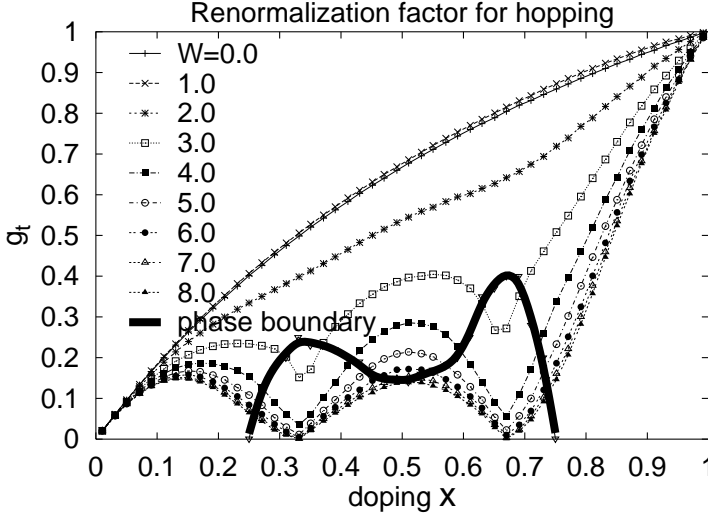


FIG. 3: Jastrow-Gutzwiller renormalization factor for hopping, Eq. (7), as a function of doping for a number of fixed W . Evaluations are done via classical Monte Carlo study of the lattice gas system. The dark thick line delineates the phases of Ψ_{JG} . The $\sqrt{3} \times \sqrt{3}$ phase lies below the thick line and in this region the exhibited g_t is averaged over all bonds.

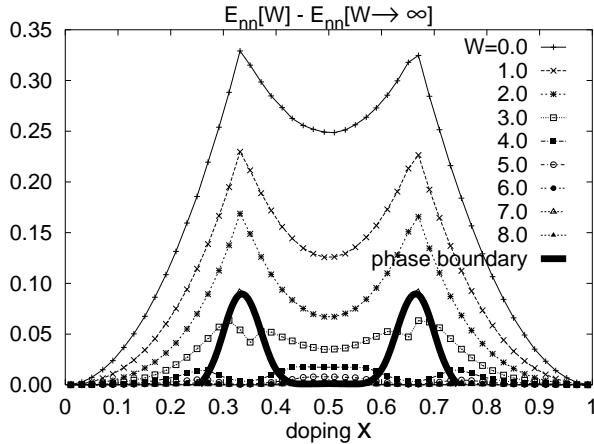


FIG. 4: Nearest-neighbor repulsion energy per site, referenced to the $W \rightarrow \infty$ value. The $\sqrt{3} \times \sqrt{3}$ charge ordered phases of Ψ_{JG} lie below the thick line.

ergy $E_{nn} = \sum_{\langle ij \rangle} \langle n_i n_j \rangle$ per site (cf. Eq. 8), which we reference to the minimal possible repulsion energy at a given density: $E_{nn, W \rightarrow \infty} = 0$ for $\rho \in [0, 1/3]$, $3\rho - 1$ for $\rho \in [1/3, 2/3]$, and $6\rho - 3$ for $\rho \in [2/3, 1]$. When plotted in this way, the result is symmetric with respect to $\rho = 0.5$ due to classical particle-hole symmetry. Again, the classical phase boundary is sketched with a thick dark line. Observe that the curves with $W > 5$ give almost complete “minimum-nearest-neighbor” projection.

With this data, and also using the free-fermion $\langle \hat{H}_t \rangle_0(x)$ (not shown), we can optimize the full tV Hamiltonian in this renormalized meanfield procedure for Ψ_{JG} . The resulting “phase diagram” can be seen in Fig. 5:

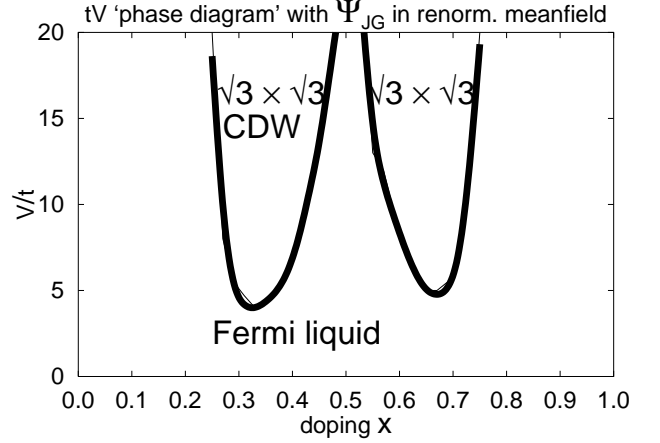


FIG. 5: “Phase diagram” obtained by optimizing the tV Hamiltonian over the JG wavefunctions. The different “phases” correspond to the difference in the physical properties of Ψ_{JG} as a function of W . Calculations are performed in the renormalized meanfield approximation using the data of Figs. 3, 4, and the free fermion $\langle \hat{H}_t \rangle_0(x)$. The phase diagram is not expected to be symmetric relative to V — cf. Fig. 3. The observed rough symmetry is due to compensating tendencies in $g_t(x)$ and $\langle \hat{H}_t \rangle_0(x)$ that make the actual kinetic energy “more symmetric” relative to $x = 0.5$.

For each doping $x \in [0.27, 0.73]$ we show the “critical” V/t that drives the optimal W into the regime with the $\sqrt{3} \times \sqrt{3}$ order.

We emphasize that this “phase diagram” is for the optimized Jastrow-Gutzwiller wavefunction only; in particular, the exhibited “phase transition” corresponds to the transition in the properties of Ψ_{JG} as a function of parameter W . It need not correspond to the actual phase diagram of the tV Hamiltonian. It is exhibited here primarily to delineate the regimes where the JG renormalized Fermi liquid can adequately describe the tV model energetics, and also where such description is no longer possible. In the latter case, one should seriously examine other physical states paying particular attention to charge order. Whether the JG wavefunction in its $\sqrt{3} \times \sqrt{3}$ phase can adequately describe the possible charge ordering in the system is a separate question that requires a detailed study. We will discuss this more specifically in the next section. Here we only note that it is rather fortuitous that our trial wavefunction with a single variational parameter exhibits two phases, and the initially “unexpected” charge-ordered state should be treated with great caution.

We now return to the main question of this work—the bandwidth suppression due to nearest neighbor repulsion. Again, consider Fig. 3. A conservative approach is to insist that we consider Fermi liquid wavefunctions only. In this case, we should disregard the data points that end up in the charge ordered phase. We still see that there can be significant renormalizations by a factor of three to five relative to the bare hopping amplitude even remaining in

the Fermi liquid state. For a fixed W , these renormalizations are strongest near the commensurate $1/3$ and $2/3$ fillings, and weakest near $x = 1/2$. Also, as can be implied from the “phase diagram”, the effect of the nearest neighbor repulsion V is strongest near $x = 1/3, 2/3$.

On the other hand, if we are to take the Jastrow-Gutzwiller $\sqrt{3} \times \sqrt{3}$ density wave regime seriously, there can be even stronger renormalizations of the hopping energy, particularly near the commensurate densities. As we will suggest in the following more specific discussion of the CDW regime, the entire picture provided by Fig. 3 including the data under the phase boundary is indeed useful, but may require some less important adjustments. This is because in the $\sqrt{3} \times \sqrt{3}$ regime the charge order is such that there remain mobile (even if strongly constrained) carriers; there is no charge gap since there is no nesting for the considered dopings. The Jastrow-Gutzwiller wavefunction and the above renormalized meanfield treatment also capture this, and give a first useful guess on the effect of charge order on the fermion kinetic energy.

V. ENERGETICS WITH Ψ_{JG} : VMC STUDY. POSSIBLE CDW.

We now consider the tV model energetics in more detail for specific $x = 0.70$ and $x = 0.35$. These values are relevant for the unhydrated and hydrated Na_xCoO_2 . The evaluations with the trial wavefunctions are done essentially exactly using VMC.^{22,25} This more concrete setting will allow us to discuss some robust features that emerge from our study vs the specifics of the particular Hamiltonian used to model charge frustration. Since an accurate treatment of the CDW states may depend on specific details, the present discussion is only intended to give a flavor of the possibilities that should be considered.

A. Doping $x = 0.70$

Figure 6 shows expectation values of the two parts of the tV Hamiltonian in the Jastrow-Gutzwiller wavefunction for varying W evaluated using VMC. It also shows the renormalized meanfield approximation to these expectation values. As mentioned in the previous section, this approximation is indeed fairly accurate and can be taken seriously. Since we will be comparing several trial states, we will use only VMC results in this section.

At this particle density we have $W_c \approx 3.3$ in the corresponding lattice gas system. Notice that near W_c the repulsion energy drops quickly and essentially all the way to zero, similar to the transition in the classical system. This is because it is possible to completely satisfy the repulsion energy by arranging charges so that there are no nearest neighbors. Also, such arrangements still allow some fermion hopping, so there remains nonzero kinetic energy gain even for very large W .

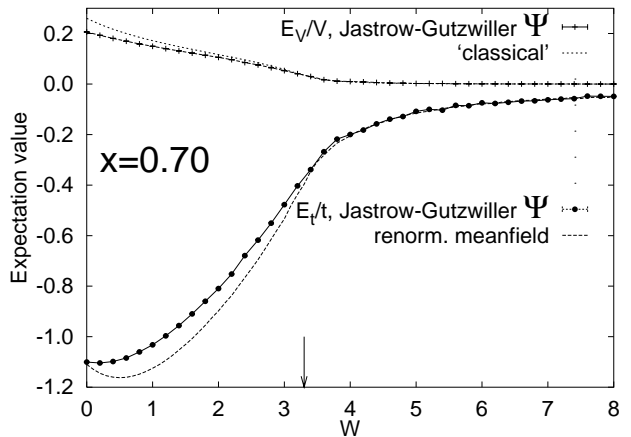


FIG. 6: Expectation values of the hopping and nearest neighbor repulsion energies in the Jastrow-Gutzwiller wavefunction at doping $x = 0.70$ (fermion density $\rho = 0.3$). We also show the corresponding renormalized meanfield values. Vertical arrow near $W_c \approx 3.3$ indicates the transition point in the classical lattice gas system.

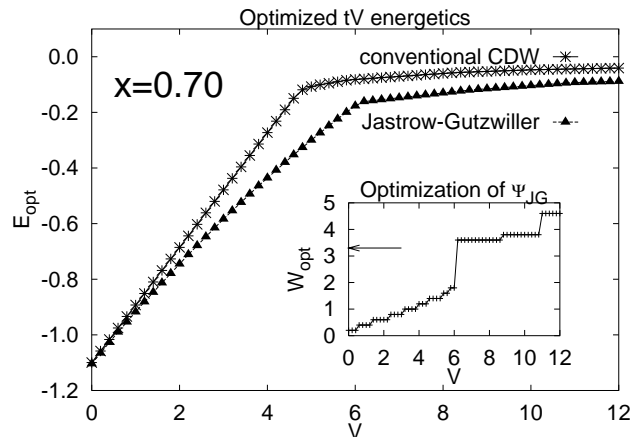


FIG. 7: Optimization of the tV Hamiltonian over Jastrow-Gutzwiller and conventional CDW trial wavefunctions. Inset shows the optimal W_{opt} for the Jastrow-Gutzwiller wavefunction; arrow indicates the critical $W_c \approx 3.3$ in the corresponding classical lattice gas system.

Using the above data, we can optimize the total energy for different values of V/t . The result is indicated in Fig. 7. For $V/t \lesssim 6.0$, the optimal W_{opt} remains $\lesssim 2.0$ and the wavefunction is metallic with relatively weak renormalizations. For larger V/t , the optimal W_{opt} jumps to the $\sqrt{3} \times \sqrt{3}$ ordered side, and Ψ_{JG} has the corresponding density wave order. Note that the optimal W_{opt} remains fairly close to the critical value. In this way, while the repulsion energy is almost completely satisfied, the system still gains from some of the original kinetic energy.

We now discuss the regime of large V , where the Jastrow-Gutzwiller energetics suggests charge ordering. First, it is instructive to compare this with the energetics

ics in a more conventional CDW trial state. Such a state is obtained, for example, by considering a CDW mean-field Hamiltonian

$$H_{\text{CDW}}^{\text{mf}} = - \sum_{\langle ij \rangle} (t_{ij} c_{i\sigma}^\dagger c_{j\sigma} + \text{h.c.}) - \sum_i 2\Delta_{\mathbf{Q}} \cos(\mathbf{Q} \cdot \mathbf{r}_i) \hat{n}_i. \quad (9)$$

$\Delta_{\mathbf{Q}} \equiv \Delta_{\text{CDW}}(\mathbf{Q})$ is a CDW order parameter at the ordering wavevector \mathbf{Q} . Here, Δ_{CDW} serves as a variational parameter for the trial wavefunction. In the $\sqrt{3} \times \sqrt{3}$ phase, the trial H_{CDW} has onsite potential -2Δ on the preferred A sublattice and $+\Delta$ on the B and C sublattices of the triangular lattice. The trial wavefunction is obtained by Gutzwiller projection of the meanfield ground state.

The optimized tV energetics for such more conventional CDW wavefunction is also shown in Fig. 7. For $V/t \lesssim 4.5$ the optimal wavefunction has $\Delta_{\text{CDW}} \approx 0$, but develops strong CDW order for larger V/t . In this conventional CDW state at this filling, we have a coexistence of the charge order and Fermi liquid.

From Fig. 7, we see that the JG wavefunction performs significantly better than the conventional CDW wavefunction. This is simple for the metallic side, since the JG wavefunction has an additional variational parameter to optimize local correlations compared to the plain metallic state with $\Delta_{\text{CDW}} = 0$. On the other hand, on the charge-ordered side the Jastrow-Gutzwiller wavefunction performs better almost entirely due to better kinetic energy. As discussed earlier, the JG state retains some of the metallic kinetic energy even in the large W limit. At the same time, the conventional CDW wavefunction localizes the fermions to the A sublattice very strongly and loses essentially all kinetic energy: in the limit of large V , the optimal $\Delta_{\text{CDW}} \sim V$ and the optimal total energy is $\sim -t^2/V$. Even though the lowest band remains only partially filled, its bandwidth goes to zero in the limit of large Δ_{CDW} .

Thus, we conclude that the Jastrow-Gutzwiller wavefunction with the $\sqrt{3} \times \sqrt{3}$ order performs fairly well for large V . However, this is by no means the end of the story even for the tV model. The most serious reservation here is that we have not explored other competing states in the system for large V . We will not address this. We still hope that our approach captures the relevant local energetics in the system.

In the present context, we can explore the energetics of the $\sqrt{3} \times \sqrt{3}$ ordering more systematically. As discussed, the complete minimum-nearest-neighbor projection leads to the $\sqrt{3} \times \sqrt{3}$ order. For $\rho < 1/3$, we essentially have charges living on the A sublattice only and moving primarily via $A - B - A$ or $A - C - A$ routes, while the bonds $B - C$ are rarely used (see Fig. 8). In the above, we were projecting the uniform free fermion triangular lattice hopping ground state, while it is clear that in the resulting charge ordered state the hops $B - C$ are poorly utilized, and more generally the kinetic energy—the driving force for uniformity—is less important. In the $\sqrt{3} \times \sqrt{3}$ regime, it then seems more appropriate to

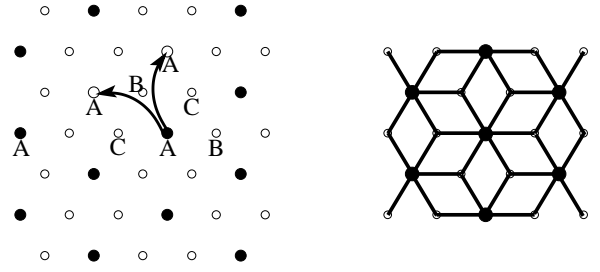


FIG. 8: a) Schematics of the $\sqrt{3} \times \sqrt{3}$ charge order for $\rho < 1/3$. Charges occupy the A sublattice and spend very little time on the B and C sublattices. The remaining empty A sites can be utilized for charge hopping. There is an intermediate repulsion energy cost of V to move an isolated such site, but no such cost for two neighboring empty A -sites as shown in the figure. b) Dice lattice hopping ansatz motivated by the observation that hops $B-C$ are rarely used.

project a hopping state with strong $A - B$ and $A - C$ hopping amplitudes and weak $B - C$ hops. The limiting case is the dice lattice hopping shown in Fig. 8b; the six-coordinated sites are the A sites, while the three-coordinated sites are the B and C sites. The dice hopping state by construction has $\sqrt{3} \times \sqrt{3}$ order. It is easy to verify that in the lowest band one half of the fermion density is located on the A sublattice. Clearly, this has better repulsion energy than the triangular hopping state. To further optimize the nearest neighbor correlations, we can introduce a Jastrow weighting as for the uniform hopping state (note that in the dice case the classical lattice gas transition is no longer relevant since the charge system has the $\sqrt{3} \times \sqrt{3}$ order from the outset). The optimized tV energetics is shown in Fig. 9, and we indeed find that the dice hopping ansatz is somewhat better than the uniform state.

Finally, we should point out that we have completely ignored the spin physics by considering only unpolarized wavefunctions. It should be clear that since the bandwidth becomes so narrow, there will be significant degeneracy—on the tV energy scale—in the spin sector. This degeneracy will be resolved in some way or other at lower energy scale, and the details will depend largely on the specifics of the microscopic Hamiltonian. As an example, trying out spin-polarized Jastrow-Gutzwiller wavefunctions in the tV Hamiltonian, we find that in the charge-ordered regime the fully polarized wavefunction performs only slightly worse than the unpolarized one. For the dice hopping ansatz, on the other hand, the spin-polarized wavefunction performs better than the unpolarized one. One can get some feeling of the slight differences by examining Fig. 9. Such itinerant ferromagnet tendencies become even more pronounced at lower fermion density (higher x).

After the presented detail, it should be clear that the energetics can be rather subtle and model dependent, particularly in the charge order regime. We now want to separate out which features are more robust than the

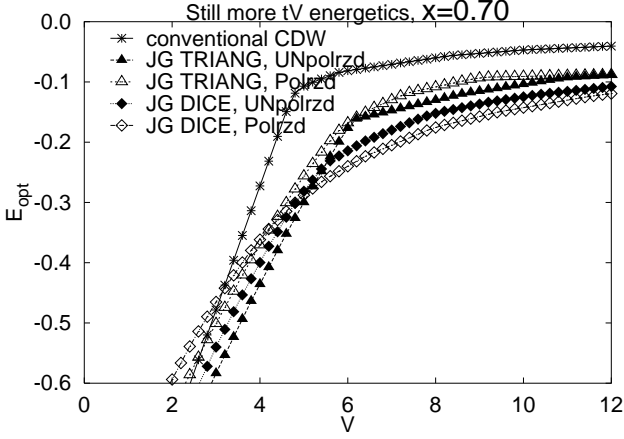


FIG. 9: This is a blow-up of Fig. 7 focusing on the $\sqrt{3} \times \sqrt{3}$ regime and showing additional Jastrow-Gutzwiller type trial wavefunctions for the tV Hamiltonian. Besides the unpolarized triangular lattice hopping ansatz, we also show the optimized energetics for the corresponding fully polarized state, and also for the dice lattice hopping ansatz.

above specifics. This is important since at present we do not have a good knowledge of the microscopic Hamiltonian in the Na_xCoO_2 system.

First of all, we conclude that there can be significant renormalizations in the metallic wavefunction. The hopping can be effectively suppressed roughly by a factor of three (see Fig. 6), with the wavefunction retaining its Fermi liquid character. The achievable Fermi liquid renormalizations may be even larger if we include further neighbor repulsion, since this will frustrate the $\sqrt{3} \times \sqrt{3}$ charge order and give more parameter space to the liquid state with uniform charge distribution. As long as the system remains uniform, this is not sensitive to the microscopics. (At this local “high energy” level of analysis we completely disregard the low energy instabilities of the resulting Fermi liquid state.)

Our second observation is about the nature of possible charge orders in such strongly frustrated system. Our JG wavefunctions offer an interesting possibility of essentially satisfying the nearest neighbor Coulomb repulsion while retaining some kinetic energy gain and metallicity. Projecting the triangular or dice lattice hopping is merely a detail of how the quantum tunneling is put into the wavefunction, but the overall picture of the resulting state is the same. Whether such state is energetically favorable compared with other competing states requires a more detailed study.

Finally, we expect that the spin dynamics is highly degenerate in such charge frustrated systems, and its ultimate fate is resolved only at much lower energy scales.

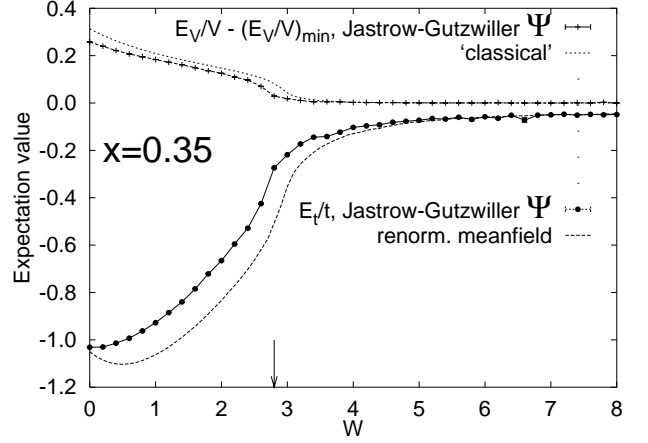


FIG. 10: This is similar to Fig. 6, but for doping $x = 0.35$ (fermion density $\rho = 0.65$). The repulsion energy is referenced to the minimal repulsion energy. At this density, $W_c \approx 2.8$.

B. Doping $x=0.35$

We now summarize similar tV study at $x = 0.35$. This is of interest for the hydrated compound $\text{Na}_{0.35}\text{CoO}_2 \cdot 1.3\text{H}_2\text{O}$ that was found to exhibit superconductivity.

Figure 10 shows the expectation values of the kinetic and nearest neighbor repulsion energies in the Ψ_{JG} evaluated using VMC. The repulsion energy is referenced to the minimal repulsion energy at this density [$E_{nn,min} = V(3\rho - 1)$ per site; cf. Fig. 4]. The renormalized meanfield approximation is also shown and is fairly accurate.

The result of the wavefunction optimization for the tV Hamiltonian is shown in Fig. 11. For $V/t \lesssim 4.2$, the optimal W_{opt} remains $\lesssim 1.5$; the wavefunction is metallic with weak renormalizations. For larger V/t , the optimal Ψ_{JG} jumps to the $\sqrt{3} \times \sqrt{3}$ ordered side; however, the optimal W_{opt} remains fairly close to $W_c \approx 2.8$, and the system retains significant part of the original kinetic energy.

Turning to the regime of large V , we consider also the more familiar CDW trial state obtained from the meanfield Hamiltonian Eq. (9). The optimized energetics with such conventional CDW wavefunction is also shown in Fig. 11. The optimal Δ_{CDW} remains close to zero for $V \lesssim 3$, but becomes significant and negative for larger V . We now observe that in the regime with the putative $\sqrt{3} \times \sqrt{3}$ charge order both the JG wavefunction and the meanfield CDW wavefunction give very close optimal energies. This is also true for the individual t and V parts, suggesting that the Jastrow-Gutzwiller and conventional CDW wavefunctions give in fact essentially the same physical state.

This can be understood by examining the meanfield CDW state. For $\Delta_{\text{CDW}} < 0$ the B and C sublattices are preferentially occupied, while the A sublattice is preferentially empty. In this case, the lower two meanfield bands retain much of the original bandwidth even in the limit of large Δ_{CDW} . This is because the B and C

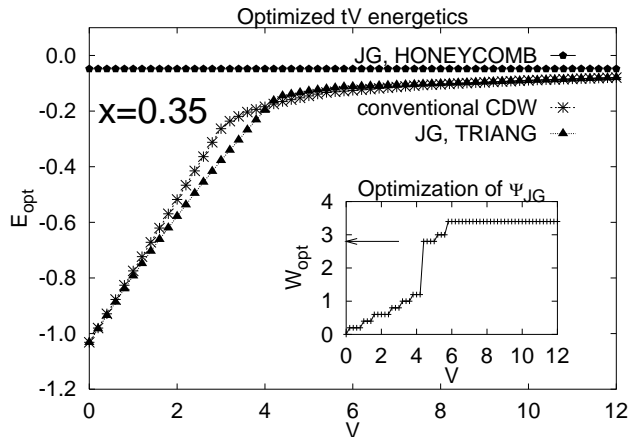


FIG. 11: Optimization of the tV Hamiltonian over Jastrow-Gutzwiller and conventional CDW trial wavefunctions at $x = 0.35$ (cf. Fig. 7). We also show the result for Jastrow-Gutzwiller honeycomb hopping ansatz.

sites form a connected honeycomb lattice, and for large Δ_{CDW} the two bands correspond essentially to hopping on this lattice. The physical state is now obtained by the Gutzwiller projection of this free fermion honeycomb lattice hopping state. But this is also roughly the picture of the Jastrow-Gutzwiller wavefunction in the $\sqrt{3} \times \sqrt{3}$ regime for this density.

The above suggests that we also try projecting honeycomb hopping ansatz, since it better utilizes the $B - C$ hops. However, for the range of V/t studied here, the uniform triangular hopping ansatz performs better, primarily since it manages to retain some of the $A - B$ and $A - C$ hopping energy. This completes our exploration of the $\sqrt{3} \times \sqrt{3}$ order.

Finally, we note that at this high fermion density $\rho = 0.65$, unlike the case with $\rho = 0.30$, the spin degeneracy does not occur, and the unpolarized wavefunctions are always better.

To summarize, the local energetics of the tV model at $x = 0.35$ is well captured by either the renormalized Fermi liquid, or the $\sqrt{3} \times \sqrt{3}$ charge ordered state, depending on the value of V/t . The $\sqrt{3} \times \sqrt{3}$ state also has mobile fermions occupying primarily the honeycomb sublattice (of the original triangular lattice); however, since the fermion density is close to complete covering of the honeycomb lattice, the fermion hopping is strongly suppressed.

Again, the ultimate fate of the Fermi liquid (or the liquid part in the $\sqrt{3} \times \sqrt{3}$ regime) is resolved only at lower energies. In the following section we study the superconducting instability due to the J term, and whether the RVB superconductivity can be significantly enhanced by the discussed strong kinetic energy suppression.

VI. RVB SUPERCONDUCTIVITY: RESURRECTION NEAR $x = 1/3$?

We now turn to the issue of RVB superconductivity due to the antiferromagnetic spin interaction at dopings $0 < x < 0.4$. In the context of the triangular lattice tJ model, this was considered by several authors.^{17,18,19,26,27} These studies predict $d + id$ superconductivity. As expected for such RVB scenario, the superconductivity is strongest (relative to the metallic state) near half filling $x = 0$, where the charge mobility is very low. Away from half-filling at moderate dopings, the need to satisfy the kinetic energy of the carriers leads to strong suppression of the superconductivity. As pointed out in Ref. 19 and discussed further below, the experimentally observed superconductivity at doping $x = 0.35$ represents a significant problem to this scenario: If one uses the LDA bandwidth to estimate $|t_{\text{bare}}| \approx 50 - 100$ meV, and takes the hopping integral sign as in this work, and makes a reasonable guess $J \sim 10$ to 20 meV, the resulting RVB superconductivity is vanishingly weak for this doping and would not be observed.

As discussed above—cf. Fig. 3—charge frustration can lead to strong suppression of the effective hopping amplitude t_{eff} , even for larger doping. Here we study whether this suppression can be strong enough to resurrect the superconductivity at $x = 0.35$. Figure 3 also suggests that the region near $x = 1/3$ is special in that it allows the strongest such renormalizations, with or without the charge ordering. As discussed earlier, this is because the charge system is most sensitive to the further neighbor interactions near this commensurate doping. On the other hand, when the superconductivity is weak, the transition temperature is exponentially sensitive to the effective hopping amplitude (see below). Thus, we may speculate about the possibility of a small superconducting dome around this special doping due to charge correlation (possibly, charge ordering).

The physics treatment presented below is very schematic. We will essentially think only in terms of the renormalized couplings and ignore the fact that the underlying “liquid” state may be charge-ordered. This is done to get a rough feeling as to whether the suggested scenario can work at all. If the superconductivity near $x = 1/3$ can reappear only in the charge-ordered region, the obtained insight is still useful and may suggest a more careful treatment. For example, the charge order may be suppressed by longer range repulsion. Another possibility is that a more accurate treatment may lead to short range charge order for intermediate coupling which shares the same kinetic energy suppression.

We first summarize the standard RVB meanfield for the pure tJ model. We formulate this meanfield as an approximate variational procedure.^{21,22,26} This is particularly convenient for the present work, which also takes the variational wavefunction perspective.

To study the possibility of singlet superconductivity,

we consider “trial” Hamiltonian

$$H_{\text{trial}} = \sum_{ij} \left[-\chi_{ij} c_{i\sigma}^\dagger c_{j\sigma} - (\Delta_{ij} c_{i\uparrow}^\dagger c_{j\downarrow}^\dagger + \text{h.c.}) \right] - \sum_i \mu \left[c_{i\sigma}^\dagger c_{i\sigma} - (1-x) \right],$$

with $\chi_{ji} = \chi_{ij}^*$, $\Delta_{ji} = \Delta_{ij}$. For each such trial Hamiltonian, we obtain the corresponding ground state $|\Psi_0\rangle$. In the meanfield, we ignore the no-double-occupancy con-

straint and only require the average density to be correctly $\langle c_{i\sigma}^\dagger c_{i\sigma} \rangle = 1-x$, which is achieved by tuning the chemical potential μ . Going beyond the meanfield, the physical wavefunction is obtained by Gutzwiller projection.

As discussed at length earlier, we can approximate the expectation value of the tJ Hamiltonian in the physical wavefunction by proper renormalizations of the meanfield values:

$$\frac{\langle \Psi_G | \hat{H}_{tJ} | \Psi_G \rangle}{\langle \Psi_G | \Psi_G \rangle} \approx g_t \frac{\langle \Psi_0 | \hat{H}_t | \Psi_0 \rangle}{\langle \Psi_0 | \Psi_0 \rangle} + g_J \frac{\langle \Psi_0 | \hat{H}_J | \Psi_0 \rangle}{\langle \Psi_0 | \Psi_0 \rangle} = -g_t \sum_{\langle ij \rangle} t_{ij} \langle c_{i\sigma}^\dagger c_{j\sigma} \rangle + \text{c.c.} - g_J \sum_{\langle ij \rangle} \frac{3J_{ij}}{8} \left[|\langle c_{i\sigma}^\dagger c_{j\sigma} \rangle|^2 + |\langle c_{\sigma\sigma'}^\dagger c_{i\sigma}^\dagger c_{j\sigma'}^\dagger \rangle|^2 \right]. \quad (10)$$

The hopping renormalization factor is given by Eq. (3), while for the Heisenberg exchange we have^{21,22}

$$g_J = \frac{4}{(1+x)^2}. \quad (11)$$

These estimates follow essentially from the no-double-occupancy configuration constraints, and do not depend on the details of the preprojected state as long as it is spatially uniform. Also, they give numerical results that are fairly close to the actual evaluations with the projected wavefunctions, as discussed earlier. The above is precisely the renormalized meanfield formulation of Refs. 21,22,26. The slave boson meanfield of Ref. 19 uses instead $g_t = x$ and $g_J = 1$, so their numerical values are somewhat different.

In this formulation, only the ratio Δ/χ is meaningful. A convenient procedure to minimize Eq. (10) is to minimize instead the so called meanfield Hamiltonian

$$\hat{H}_{\text{mf}} = \sum_{\langle ij \rangle} \frac{8}{3g_s J_{ij}} \left[|\chi_{ij} - g_t t_{ij}|^2 + |\Delta_{ij}|^2 \right] + \hat{H}_{\text{trial}}.$$

By standard arguments, the global minimum of the meanfield Hamiltonian is also the minimum of the trial expectation value Eq. (10). In this formulation, the optimal χ and Δ each obtain physical scale as set by t and J . Thus, we can get a rough idea about the quasi-particle spectrum above the ground state by considering the meanfield excitation spectrum, which now has proper physical scale. In particular, the optimal Δ gives a physical measure of the strength of superconductivity.

The self-consistency conditions read

$$\chi_{ij}^* = g_t t_{ij} + \frac{3g_s J_{ij}}{8} \langle c_{i\sigma}^\dagger c_{j\sigma} \rangle, \quad (12)$$

$$\Delta_{ij}^* = \frac{3g_s J_{ij}}{8} \langle c_{\sigma\sigma'}^\dagger c_{i\sigma}^\dagger c_{j\sigma'}^\dagger \rangle. \quad (13)$$

From now on, we specialize to the $d+id$ superconductor

ansatz:

$$\Delta_{e_1} = \Delta; \quad \Delta_{e_2} = \Delta e^{i2\pi/3}; \quad \Delta_{e_3} = \Delta e^{i4\pi/3}. \quad (14)$$

Here $e_1 = \hat{x}$, $e_2 = \frac{1}{2}\hat{x} + \frac{\sqrt{3}}{2}\hat{y}$, and $e_3 = e_2 - e_1$ are the unit triangular lattice vectors. There is strong evidence that this state wins the tJ model energetics for the considered dopings, at least on the meanfield level.^{17,18,19,26,27}

We give the results for $t = 3J$ and $t = 5J$. This is somewhat different from the cited $t = 5 - 10J$ values.¹⁹ At the moment, there is significant uncertainty in the precise microscopic model, while the superconductivity energy scale is exponentially sensitive to the microscopic values and to numerical constants in the theory. The $t = 3J$ results make the demonstration of principle more dramatic. A similar, but weaker, effect is seen for $t = 5J$.

The optimal Δ in units of J is shown as a function of doping in Fig. 12. For weak J , the optimal Δ is given by a BCS-like formula (see Appendix A for details)

$$\Delta \sim t_{\text{eff}} e^{-c t_{\text{eff}} / J_{\text{eff}}} \quad (15)$$

with some numerical constant $c = c(x)$ and $t_{\text{eff}} = g_t t$, $J_{\text{eff}} = g_J J$. The effective mobility of charges increases with doping $t_{\text{eff}} \sim xt$, and this leads to the observed very quick drop of Δ .

Figure 12 also shows two other physical measures of the strength of superconductivity. One is the meanfield T_c defined here as the transition temperature for the finite temperature optimization of the meanfield Hamiltonian H_{mf} .

The other measure is obtained by considering the condensation energy of the superconducting state. This is defined as the energy gain in the optimal superconducting state relative to the Fermi liquid state ($\Delta = 0$). For small Δ , the condensation energy is expected to scale as $E_{\text{cond}} \sim \Delta^2 / t_{\text{eff}}$; to compare with Δ in Fig. 12, we plot instead $(E_{\text{cond}} J)^{1/2}$.

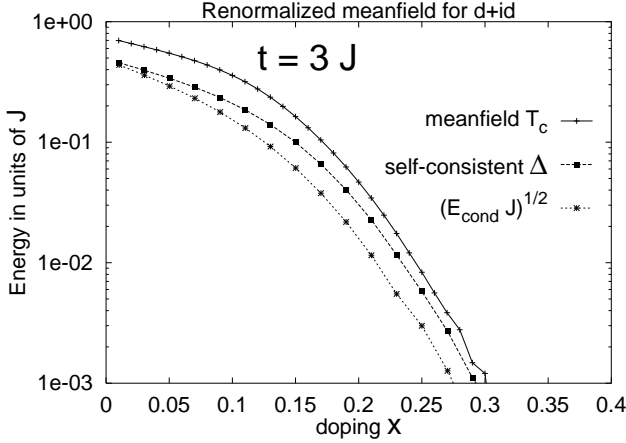


FIG. 12: Renormalized meanfield results for the $d + id$ superconducting state for $t = 3J$. We show the meanfield T_c , the optimal Δ , and the square root of the condensation energy E_{cond} . The energy scale is the bare J ; note the logarithmic scale for the energy.

From Fig. 12, these measures all trail each other. The figure has been somewhat arbitrarily cutoff at $10^{-3}J$. For $J \sim 20\text{meV}$, any T_c or Δ below this scale would not be observed in the experiments. Note the precipitous drop in the strength of superconductivity for $x \gtrsim 0.20$. There is simply no hope for it surviving to the experimentally observed $x = 0.35$ in this setting.

We remark here that a direct VMC study must see the condensation energy to establish the ground state Δ . Since E_{cond} is extremely small, such studies become impractical. This is where the renormalized meanfield procedure becomes very useful.

Let us now return to the tJV model with strong nearest neighbor repulsion. We think roughly as follows. The dominant t and V parts can be satisfied as above by the appropriate Jastrow weighting of charge configurations in our trial wavefunctions. As discussed earlier, the effect of the Jastrow factor can be conveniently described by the corresponding renormalizations of the hopping amplitude g_t (Eq. 7 and Fig. 3) and the Heisenberg exchange g_J . The latter is approximated by

$$g_J = \frac{\langle\langle \delta(n_i - 1)\delta(n_j - 1) \rangle\rangle}{[\rho(1 - \rho/2)]^2}, \quad (16)$$

and is plotted in Fig. 13 (cf. discussion following Eq. 7). As long as the charge distribution remains uniform, these renormalizations capture the main effect of the nearest neighbor correlations built in by the Jastrow factor.

Thus, for each doping level x and the Jastrow suppression strength W , we can estimate the corresponding t_{eff} , J_{eff} , and then the optimal Δ . The latter is our main measure of the superconductivity strength and is shown in Fig. 14. The $W = 0$ line is the same as in Fig. 12, while the $W = 8$ corresponds essentially to the minimum-nearest-neighbor projection. Again, the dark

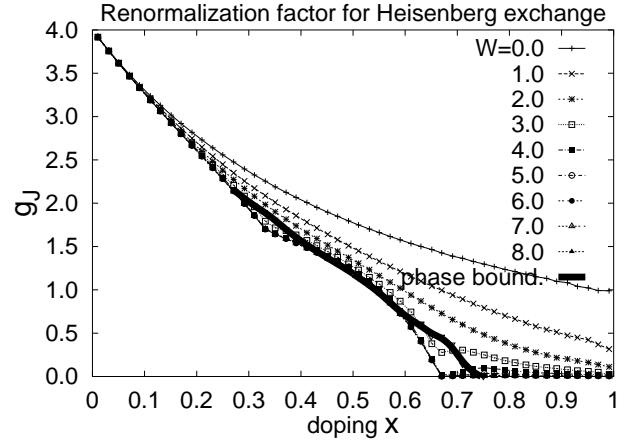


FIG. 13: Jastrow-Gutzwiller renormalization factor for the Heisenberg exchange as a function of doping for a number of fixed W (cf Figs. 3,4). In the $\sqrt{3} \times \sqrt{3}$ phase (data points below the thick dark line), the exhibited g_J is averaged over all bonds.

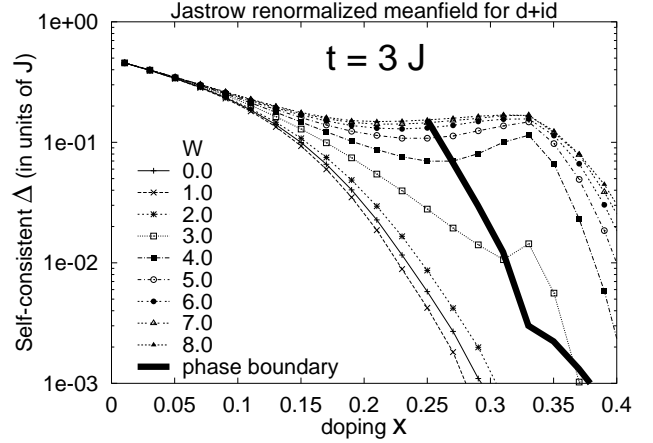


FIG. 14: Renormalized meanfield for the Jastrow-weighted $d + id$ superconducting state for $t = 3J$ (cf. Fig. 12). We show the self-consistent Δ as the measure of the superconductivity strength (T_c plots look very similar). The dark thick line corresponds to the phase boundary of the Jastrow weight (cf. Figs. 2,3,13) — the maximum enhancement of the superconductivity while remaining in the uniform phase.

thick line corresponds to the phase boundary of the Jastrow weight. For $x > 0.27$ all points above this line have the $\sqrt{3} \times \sqrt{3}$ charge order. These are obtained by using the corresponding formal renormalization factors and the above prescription, even though this violates the initial motivation coming from a uniform renormalized liquid picture. As emphasized earlier, the precise energetics in this regime likely requires a more careful treatment. However, we expect that even such simplistic analysis in the $\sqrt{3} \times \sqrt{3}$ regime gives a reasonable first guidance on how the role of the kinetic energy can be suppressed by possible charge ordering in the system.

Our tentative conclusion from Fig. 14 is that for $t = 3J$

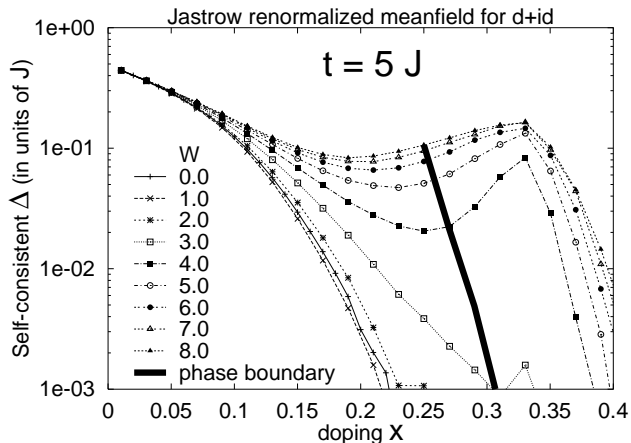


FIG. 15: This is the same as Fig. 14, but for $t = 5J$.

the considered nearest neighbor Jastrow renormalizations that leave the underlying liquid wavefunction in the pure Fermi liquid state are borderline sufficient to explain the superconductivity near $x = 1/3$. One should of course judge this critically because of the exponential sensitivity to the actual value of the ratio $t_{\text{eff}}/J_{\text{eff}}$, Eq. (15). The trend for increasing t/J can be seen by comparing $t = 3J$ Fig. 14 and $t = 5J$ Fig. 15.

We speculate that in $\text{Na}_x\text{CoO}_2 \cdot 1.3\text{H}_2\text{O}$ the actual situation is qualitatively close to the curve with $W = 3$ in Fig 14, which near $x = 1/3$ roughly corresponds to the critical strongly correlated liquid of the nearest neighbor Jastrow weight (cf. Figs. 2,3). This curve may lie inside the liquid phase for longer ranged Jastrow weight. Another possibility is that only short range charge order is developed for intermediate coupling. One thing should be clear from Figs. 14,15: there can indeed be significant enhancement—one to two orders of magnitude—in the superconductivity scale due to the kinetic energy suppression in the charge-correlated liquid. Because the charge system is most responsive near the commensurate $x = 1/3$, this enhancement may be strongest near this doping, which may explain the experimentally suggested³ superconducting “dome” around $x = 1/3$. However, we note that even for $W = 3$, Δ in Fig. 14 shows only a shallow maximum near $x = 1/3$. A possible explanation of the experiment is that x significantly less than $1/3$ is not achievable due to chemical reasons and superconductivity is simply cut-off. Again, the important message we draw from Fig. 14 is the possibility of pushing T_c up to an observable level near $x = 1/3$.

Finally, if we continue the theory into the Jastrow $\sqrt{3} \times \sqrt{3}$ charge order regime, the T_c enhancement may be even stronger. This is not surprising, since the charge mobility is suppressed even further in this case. Thus, our earlier analysis tells us that for $x > 1/3$ we are essentially doping a nearly half-filled honeycomb lattice. This picture also suggests some possibilities of treating the $\sqrt{3} \times \sqrt{3}$ regime more carefully, similar to our discussion in Sec. V. For example, for $x > 1/3$, we can

view the fermions as restricted primarily to the honeycomb lattice. On the other hand, the $d + id$ state wins the energetics in the original uniform triangular lattice meanfield and needs to be re-examined in the present context. The above renormalized meanfield procedure roughly corresponds to restricting the $d + id$ ansatz onto the honeycomb lattice. Of course, one should also consider other possible RVB superconductor states on the honeycomb lattice and decide which one is optimal energetically. More generally, one may want to consider triangular lattice superconducting ansatz with broken translational symmetry patterned after the $\sqrt{3} \times \sqrt{3}$ state. We are not pursuing such studies here, since it is important to first establish whether the charge ordering occurs at all in the material. If this indeed happens, the above rough considerations can give us some initial idea about the scale of the superconducting instabilities in such state.

VII. CONCLUSIONS. CONNECTION WITH EXPERIMENTS.

We conclude by stating some consequences of the discussed effects of charge frustration.

1) It will clearly be interesting to look for signs of charge order near $x = 1/3$ and $2/3$ using X-ray or neutron scattering. The conductivity is metallic and in the case of $x = 1/3$ reaches $50e^2/h$ at low temperatures.^{4,9} This suggests that long-range charge ordering is unlikely, but there may be a tendency for short-range ordering.

2) There can be strong suppression of the effective hopping amplitude due to nearest neighbor repulsion while remaining in the Fermi liquid state. The meanfield hopping amplitude $\chi_{ij} = \chi$ is given by Eq. (12) and has contributions proportional to $g_t t$ and $g_J J$. Note that in addition to the suppression of g_t (Fig. 3), g_J is also suppressed (Fig. 13), especially for $x > 0.5$.

This suppression leads to low fermion degeneracy temperature. The properties of such Fermi liquid system with $\epsilon_F \lesssim T$ are rather unusual from the perspective of the familiar metals with $\epsilon_F \gg T$ (the Fermi energy is measured from the bottom of the band, and is roughly $\epsilon_F \sim t_{\text{eff}}$).

a) In particular, the thermopower is large and saturates to the value

$$Q = -\frac{\mu}{qT} = \frac{k_B}{q} \ln \frac{2-\rho}{\rho}. \quad (17)$$

at large temperature. Note the “classical” scale $k_B/|e| = 86.2 \mu\text{V/K}$, which is in fact observed in Na_xCoO_2 .^{5,7,9} The full temperature dependence for $x = 0.70$ is shown in Fig. 16. Here and below, we use simple-minded transport theory summarized in Appendix B. From Fig. 16, the thermopower reaches one half of the maximal value for $T \approx t_{\text{eff}}$.

b) The Hall coefficient for the triangular lattice band structure has an unusual non-saturating increase with

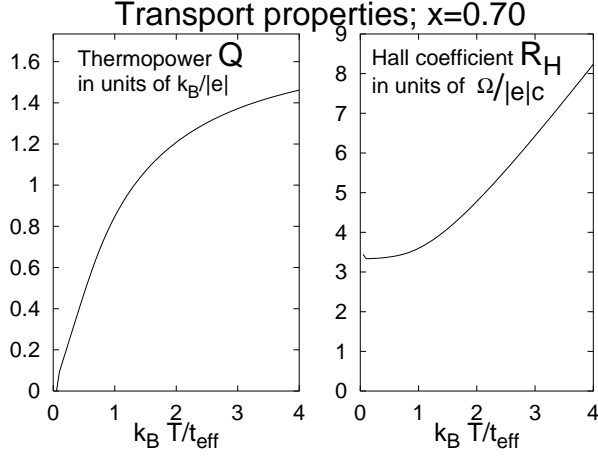


FIG. 16: Simple-minded transport theory for nondegenerate spin-1/2 Fermi gas on the triangular lattice. The thermopower is plotted in “classical” units of $k_B/|e|$, while the units for the Hall coefficient contain the three-dimensional volume per Co atom Ω .

the temperature for $T \gtrsim \epsilon_F$ as observed experimentally in Ref. 10. The limiting high temperature behavior is

$$R_H = \frac{\Omega}{qc\rho(2-\rho)} \frac{k_B T}{t_{\text{eff}}}, \quad (18)$$

where Ω is the three-dimensional volume per Co. The full temperature dependence is shown in Fig. 16; the high temperature trend sets in for $T \approx 1$ to $2 t_{\text{eff}}$. Possibility of this unusual behavior was predicted in Ref. 18 from the high temperature expansion for the tJ model (the doping dependence of the proportionality coefficient is somewhat different here). We remark that this unusual behavior is the consequence of the triangular lattice band structure only, and its origin can be traced to the presence of three-site hopping loops as detailed in Appendix B. Correlation effects per se are needed only to reduce t_{eff} below the experimental temperatures.

c) Pauli susceptibility per Co site for $T \gtrsim \epsilon_F$ becomes

$$\chi = \frac{\mu_B^2}{T} \rho(1 - \rho/2). \quad (19)$$

Note that this has a Curie-like behavior, but is somewhat smaller—by a factor of $1 - \rho/2$ —from the case of completely free spins.

3) The kinetic energy renormalizations are strongest (for fixed repulsion strength) near the commensurate $x = 1/3, 2/3$, and weakest near $x = 1/2$. This is because the system finds it easiest to order, even if only locally, near the commensurate filling, while away from commensuration much of the nearest neighbor repulsion energy cannot be avoided in any case.

Charge frustration may also be relevant for the experimental “charging” curve of Ref. 4. The observed plateaus at $x = 1/3, 2/3$ remind one of the magnetization plateaus in the frustrated triangular lattice Ising

model (related to the lattice gas with nearest neighbor repulsion as mentioned in Sec. III). Note that the bandwidth observed by heat capacity^{4,6} and by ARPES¹¹ is proportional to χ and has contributions from both $g_t t$ and $g_J J$ (see Eq. 12). On the other hand, electromagnetic response couples only to t so that the Drude weight (observable from infrared reflectivity and the superfluid density (observable via the London penetration depth in the case of superconductors) are directly proportional to g_t . These will provide a more sensitive test of the predicted dip in g_t near $x = 1/3$ and $x = 2/3$ as shown in Fig. 3. For example, it will be interesting to compare the Drude weight for $x = 1/3$ and $x = 0.5$ samples.

4) The spin physics near $x = 2/3$ is expected to be highly degenerate and complicated, and will manifest itself below the energy scale t_{eff} . In particular, the above transport pictures will likely be modified below this scale.

5) Near $x = 1/3$, whether the system prefers uniform or charge-ordered state, the correlated liquid can have further RVB superconducting instabilities. The suppression of the charge mobility serves to enhance and may even resurrect the superconductivity under a small superconducting dome around $x = 1/3$. Experiments³ observe the disappearance of the superconductivity below $x = 0.26$. However, the strongest RVB superconductivity is expected at much lower doping, and the search should be pursued more vigorously towards $x = 0$, if that is chemically possible.

Acknowledgments

The authors are grateful to A. Vishwanath, C. Honerkamp, and T. Senthil for many useful discussions, and to N. P. Ong for making experimental results available before publication. This work was supported by the National Science Foundation under grants DMR-0201069 and DMR-0213282. OIM also wants to thank his family for support during his stay in Ukraine.

APPENDIX A: DETAILS OF EQ. (15)

Eq. (15) can be understood by examining the self-consistency conditions Eq. (13). Specializing for the $d+id$ ansatz, we have

$$1 = \frac{3J_{\text{eff}}}{8} \frac{1}{N_{\text{latt}}} \sum_{\mathbf{k}} \frac{f_{d+id}(\mathbf{k})}{\sqrt{\xi_{\mathbf{k}}^2 + \Delta_{\mathbf{k}}^2}}.$$

$$f_{d+id}(\mathbf{k}) \equiv 2 \cos \mathbf{k} \cdot \mathbf{e}_1 \left(\cos \mathbf{k} \cdot \mathbf{e}_1 - \frac{1}{2} \cos \mathbf{k} \cdot \mathbf{e}_2 - \frac{1}{2} \cos \mathbf{k} \cdot \mathbf{e}_3 \right).$$

Here N_{latt} is the number of lattice sites; $\xi_{\mathbf{k}} = \epsilon_{\mathbf{k}} - \mu$ with $\epsilon_{\mathbf{k}} = -2\chi(\cos \mathbf{k} \cdot \mathbf{e}_1 + \cos \mathbf{k} \cdot \mathbf{e}_2 + \cos \mathbf{k} \cdot \mathbf{e}_3)$.

For weak superconductivity $\Delta \ll J_{\text{eff}} \lesssim t_{\text{eff}}$, following a BCS-like analysis, we obtain the following approximate

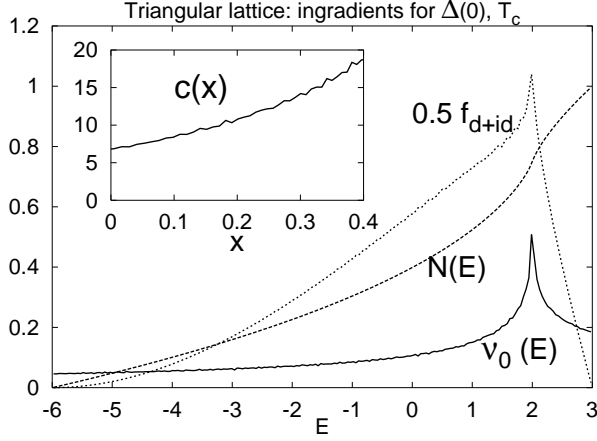


FIG. 17: Density of states per site $\nu_0(E)$ and the integrated DOS $N(E)$ for the triangular lattice band structure (unit hopping amplitude, no spin). We also show the data for the average $d + id$ wave factor \bar{f}_{d+id} at the corresponding energy cut; we plot $0.5\bar{f}_{d+id}$ to fit into the same vertical scale. To obtain the values corresponding to the particular doping x , we first locate E such that $N(E) = (1 - x)/2$. In this manner, we obtain $c(x) = 4/(3\nu_0\bar{f}_{d+id})$ plotted for the relevant range $0 < x < 0.4$ in the inset.

formula

$$\Delta = A \chi \exp\left(-\frac{4}{3\nu_0(x)\bar{f}_{d+id}(x)} \frac{\chi}{J_{\text{eff}}}\right). \quad (\text{A1})$$

A is an order one numerical constant, $\nu_0(x)$ is the triangular lattice hopping density of states per site (not including spin) at the Fermi energy corresponding to doping x , and \bar{f}_{d+id} is the $d + id$ wave factor averaged over the Fermi surface. The scale χ in front of the exponential corresponds to the energy cutoff being roughly the Fermi energy, since the pairing is over the full Fermi volume. For small J_{eff} we see from Eq. (12) that χ can be replaced by t_{eff} in (A1), yielding Eq. (15). Similar expression is obtained for the meanfield T_c .

The necessary data is shown in Fig. 17. The coefficient $c(x)$ depends rather weakly on x , and the main effect on the Δ and T_c is from the doping dependence of t_{eff} . The above approximate formula agrees fairly well with the actual meanfield calculations performed in the main text.

APPENDIX B: TRANSPORT FOR $T \lesssim \epsilon_F$

In this appendix, we summarize the simple Fermi liquid transport theory that was used to obtain Fig. 16 and Eqs. 17, 18. The main formulae can be found in standard texts.^{28,29}

a) The thermopower is given by

$$Q = \frac{L_{12}}{\sigma_{xx}}. \quad (\text{B1})$$

The kinetic coefficients are given by the integrals over the Brillouin zone

$$L_{12} = q\tau \int \frac{d^3\mathbf{k}}{4\pi^3} \left(-\frac{\partial f}{\partial \epsilon}\right) v_x(\mathbf{k}) v_x(\mathbf{k}) \frac{\epsilon(\mathbf{k}) - \mu}{T},$$

$$\sigma_{xx} = q^2\tau \int \frac{d^3\mathbf{k}}{4\pi^3} \left(-\frac{\partial f}{\partial \epsilon}\right) v_x(\mathbf{k}) v_x(\mathbf{k}).$$

Here, $f(\epsilon) = 1/(e^{\epsilon-\mu} + 1)$ is the Fermi distribution. We cite the more familiar three-dimensional expressions. When applying to Na_xCoO_2 , we specialize to the layered triangular lattice by assuming no dispersion in the \hat{z} direction. The full temperature dependence for $x = 0.70$ is shown in Fig. 16, and the limiting high-temperature behavior is given in Eq. (17).

b) In weak magnetic fields $\omega_c\tau \ll 1$, the Hall coefficient is given by

$$R_H = \frac{\sigma_H}{\sigma_{xx}\sigma_{yy}}. \quad (\text{B2})$$

σ_{xx}, σ_{yy} are the static zero field conductivities given earlier, while

$$\sigma_H = \frac{q^3\tau^2}{c} \int \frac{d^3\mathbf{k}}{4\pi^3} \left(-\frac{\partial f}{\partial \epsilon}\right) v_x(\mathbf{k}) [M_{yy}^{-1}v_x(\mathbf{k}) - M_{yx}^{-1}v_y(\mathbf{k})]. \quad (\text{B3})$$

In the last equation, $M_{\alpha\beta}^{-1}(\mathbf{k}) = \frac{\partial^2 \epsilon}{\partial k_\alpha \partial k_\beta}$ is the inverse mass tensor.

The high temperature behavior for the layered triangular lattice is given by Eq. (18). The origin of this non-saturating increase with temperature lies in the presence of triangular hopping loops. Indeed, consider the above semi-classical expression for σ_H at high temperature, and translate it from the momentum space back to the real space assuming a general hopping problem $t_{RR'}$ on a Bravais lattice. The result reads

$$\sigma_H = \frac{q^3\tau^2}{c} \left(-\frac{\partial f}{\partial \epsilon}\right) \frac{2}{\Omega} \sum_{\mathbf{R}_1, \mathbf{R}_2} t_{01}t_{12}t_{20} R_{1x}R_{2y}(\mathbf{R}_1 \times \mathbf{R}_2)_z. \quad (\text{B4})$$

Here, $-\frac{\partial f}{\partial \epsilon} \approx \rho(2 - \rho)/(4T)$, and also enters σ_{xx}, σ_{yy} ; Ω is the volume of the unit cell. The lattice hopping problem is input through the real space sum over possible hops out of the origin: $\mathbf{R}_1 \equiv \mathbf{R}_{01}, \mathbf{R}_2 \equiv \mathbf{R}_{02}$. For each triangle specified by an unordered triple of vertices $\mathbf{0}, \mathbf{R}_1, \mathbf{R}_2$, the clockwise $0 \rightarrow 1 \rightarrow 2 \rightarrow 0$ and anticlockwise $0 \rightarrow 2 \rightarrow 1 \rightarrow 0$ contributions add to $(\mathbf{R}_1 \times \mathbf{R}_2)_z^2$, i.e., a quantity of definite sign. The effect is of course strongest for the triangular lattice.

¹ K. Takada *et al.*, Nature **422**, 53 (2003).

² M. L. Foo *et al.*, cond-mat/0304464; B. Lorenz *et al.*,

- cond-mat/0304537; F. Rivadulla *et al.*, cond-mat/0304455.
- ³ R. E. Schaak, T. Klimczuk, M. L. Foo, and R. J. Cava, cond-mat/0305450.
 - ⁴ F. C. Chou, J. H. Cho, P. A. Lee, E. T. Abel, K. Matan, and Y. S. Lee, cond-mat/0306659
 - ⁵ I. Terasaki, Y. Sasago, and K. Uchinokura, Phys. Rev. B **56**, R12685 (1997).
 - ⁶ Y. Ando, N. Miyamoto, K. Segawa, T. Kawata, and I. Terasaki, Phys. Rev. B **60**, 10580 (1999).
 - ⁷ W. Koshibae, K. Tsutsui, and S. Maekawa, Phys. Rev. B **62**, 6869 (2000).
 - ⁸ R. Ray, A. Ghoshray, K. Ghoshray, and S. Nakamura, Phys. Rev. B **59**, 9454 (1999).
 - ⁹ Y. Wang, N. S. Rogado, R. J. Cava, and N. P. Ong, Nature (2003).
 - ¹⁰ Y. Wang, N. S. Rogado, R. J. Cava, and N. P. Ong, cond-mat/0305455.
 - ¹¹ M. Z. Hasan *et al.*, cond-mat/0308438.
 - ¹² G. L. Gavilano *et al.*, cond-mat/0308383.
 - ¹³ O. P. Lemmens *et al.*, cond-mat/0309186.
 - ¹⁴ M. Bruhwiler, B. Batlogg, S. M. Kazakov and J. Karpinski, cond-mat/0309311.
 - ¹⁵ D. J. Singh, Phys. Rev. B **61**, 13397 (2000).
 - ¹⁶ G. Baskaran, cond-mat/0306569.
 - ¹⁷ G. Baskaran, cond-mat/0303649.
 - ¹⁸ B. Kumar and B. S. Shastry, cond-mat/0304210.
 - ¹⁹ Q.-H. Wang, D.-H. Lee, and P. A. Lee, cond-mat/0304377.
 - ²⁰ D. Vollhardt, Rev. Mod. Phys. **56**, 99 (1984).
 - ²¹ F. C. Zhang, C. Gros, T. M. Rice, and H. Shiba, Supercond. Sci. Technol. **1**, 36 (1988).
 - ²² C. Gros, Annals Phys. (NY) **189**, 53 (1989); C. Gros, Phys. Rev. B **38**, 931 (1988).
 - ²³ M. E. Fisher, Rep. Prog. Phys. **30**, 615 (1967), and references therein; B. D. Metcalf, Phys. Lett. **45** A, 1 (1973); M. Schick, J. S. Walker, and M. Wortis, Phys. Rev. B **16**, 2205 (1977).
 - ²⁴ R. J. Baxter, J. Phys. A **13**, L61 (1981).
 - ²⁵ D. M. Ceperley, G. V. Chester and M. H. Kalos, Phys. Rev. B **16**, 3081 (1977).
 - ²⁶ M. Ogata, cond-mat/0304405.
 - ²⁷ C. Honerkamp, cond-mat/0304460.
 - ²⁸ N. Ashcroft and N. Mermin, Solid State Physics.
 - ²⁹ J. M. Ziman, Electrons and Phonons, Oxford, 1960.